Available online at www.sciencedirect.com
ScienceDirect
Applied Thermal Engineering 27 (2007) 1507–1515
Applied Thermal Engineering
www.elsevier.com/locate/apthermeng

Study of PV-Trombe wall installed in a fenestrated room with heat storage

Ji Jie *, Yi Hua, Pei Gang, Lu Jianping

Department of Thermal Science and Energy Engineering, University of Science and Technology of China, Hefei, China

Received 12 June 2006; accepted 26 September 2006
Available online 22 November 2006

Abstract

In this paper, a PV-Trombe wall (PV-TW) installed in a fenestrated room with heat storage is investigated to approach the practical application of PV-TW. Based on an updated mathematical model, theoretical simulation has been conducted for PV-TW in this case. Furthermore, field testing for this case has also been performed to validate the model, and then the simulated and experimental results are compared and found in considerably good agreement. The testing results show that a significant indoor temperature increase can be obtained in a fenestrated room with PV-TW and heat storage. Meanwhile, the experimental daily average electrical efficiency of this PV-TW can reach 10.4%.

Keywords: PV-Trombe wall; Fenestrated room; Heat storage; Simulated and experimental results; Comparison

1. Introduction

Trombe wall is a south-facing wall, blackened and covered on the exterior by glazing, and it has been used since decades for buildings with winter heating. Many theoretical and experimental studies [1–6], have even shown that indoor comfort is improved due to well-designed Trombe walls. However, most of them are of less function and look unaesthetic, which has restricted its wide application. Furthermore, BIPV (Building Integrated Photovoltaic) offers substantial opportunities for reducing building energy consumption, both through direct electricity generation, and solar thermal contributions [7,8]. Along with the development of BIPV, BIPV has been advocated worldwide for energy conservation and more effective utilization of solar energy. Thus, a novel PV-Trombe wall (PV-TW) has been presented in this situation and its basic model has been reported in our former publication [9].

Nevertheless, fenestration is generally employed in most practical rooms, which has not been considered in our previous work [9]. When a window is introduced, the modeling and simulation of a simple glass window was implemented [10], and the influence of window on the effective solar absorptance was estimated by calculating the redistribution of solar energy in rooms [11]. However, more attention was paid to how a window influenced the indoor temperature. Thus, two concepts are therefore introduced [12]: a 'solar heat gain factor' SHGF denoted by g and an 'overall heat loss coefficient' denoted by U. In other literatures, SHGF is also denoted SHGC by using 'coefficient' rather than 'factor'. These two parameters enable the instantaneous calculations of heat gains and losses in a building through various building elements, including the passive components such as direct gain, mass wall, water wall, Trombe wall, and solarium. A review of the literature about SHGF and U-value indicates rich researches, experimental and numerical. To quote some examples, the concept of SHGF and U-value were extended to size passive heating concepts as building elements for different climatic conditions in India [13]. The original U and g, in addition to the special

* Corresponding author. Tel./fax: +86 551 3601652.
E-mail address: jijie@ustc.edu.cn (J. Jie).

1359-4311/$ - see front matter © 2006 Elsevier Ltd. All rights reserved.
doi:10.1016/j.applthermaleng.2006.09.013

Nomenclature

A_{j1} surface area of zone 1 except the southern and eastern surface (m^2)
A_{j2} surface area of zone 2 except the southern and western surface (m^2)
A_S cross sectional area normal to the height direction of the air duct (m^2)
A_V area of the winter air vent (m^2)
A_{window} area of window (m^2)
C_{in}, C_{out} loss coefficients at top and bottom winter air vent, respectively
C_f fraction factor along the air duct
c_p, c_w, c_G specific heat capacity of air, wall and glass, respectively (J/kg K)
d air duct hydraulic diameter (m)
D, D_w depth of air duct, the thickness of the wall (m)
E electric power rate generated by PV cells (W/m^2)
g Gravitational acceleration, $g = 9.80665$ (m/s^2)
g_w solar heat gain factor of window
G total solar radiation on the vertical plane (W/m^2)
G_{PV} solar radiation which arrives on the PV surface (W/m^2)
h_{bo}, h_{bi} heat transfer coefficients on the southern and northern surface of the converted brick wall, respectively (W/m^2 K)
h_{co}, h_{ci} convection heat transfer coefficients on the outside surface and the inside surface of the PV glass panel (W/m^2 K)
h_{ro}, h_{ri} radiation heat transfer coefficients on out side surface and the inside surface of the PV glass panel (W/m^2 K)
h_{wo}, h_{wi} convection heat transfer coefficients on the outside surface and the inside surface of the a PV-TW wall, respectively (W/m^2 K)
h_{rwo} radiation heat transfer coefficient on the outside surface of PV-TW wall (W/m^2 K)
h_{nrwo} radiation heat transfer coefficient on the outside surface of a normal wall (W/m^2 K)
h_{nwi}, h_{nwo} convection heat transfer coefficient on the inside and outside surfaces of a normal wall, respectively (W/m^2 K)
$K_{\tau\alpha}$ a modified coefficient of transmissivity
L height of the PV-TW (m)
L_{room} depth of room (m)
$\dot{m}$ ventilated mass flow rate (kg/s)
$R_{Trombe1}$ ratio between the area of the PV-TW wall and the southern wall area of zone 1
T_{bo}, T_{bi} temperatures of the southern and northern surfaces of the converted brick wall, respectively (°C)
T_p, T_e, T_a temperatures of PV glass panel, ambient, the air in the duct, respectively (°C)
T_{wo}, T_{wi} temperatures of the outside and inside surfaces of the blackened southern wall (°C)
T_w temperatures of the PV-TW wall (°C)
T_{nwo}, T_{nwi} temperatures of the outside and inside surfaces of a normal wall (°C)
T_{out}, T_{in} temperatures of the top and bottom winter air vents (°C)
T_r indoor temperature of the PV-TW room (°C)
T_{r1}, T_{r2} air temperature of zone 1 and zone 2, respectively (°C)
T_j air temperature in the air interlayer (°C)
U_j overall heat transfer coefficient between interlayer and indoor room (W/m^2 K)
U_w overall loss coefficient of window (W/m^2 K)
V_a velocity of the air flow in the duct (m/s)
V_2 volume of zone 2 (m^3)
w width of PV-TW (m)
w_{room1}, w_{room2} width of zone 1 and zone 2, respectively (m)

Greek symbols

α_{PV}, α_{nwall}, α_{wall} absorptivity of the PV cells, the normal wall, the blackened wall, respectively
α_{WPV}, α_{NPV} equivalent absorptivities of the elements with and without PV cell on the glass panel, respectively
τ_{PV}, τ transmissivity of the PV cells' outside layers, the elements without PV cell on the glass panel, respectively
β heat expansion coefficient (K^{-1})
ε ratio of PV cell coverage
η_0 electrical efficiency at standard conditions
θ incident angle
δ_b, δ_G thickness of the converted brick wall and the glass panel (m)
ρ, ρ_G, ρ_w density of the air, glass, wall, respectively (kg/m^3)
ξ_1, ξ_2, ξ_3 emissivity factors
λ_G, λ_w thermal conductivity of glass, wall, respectively (W/m K)

U_{vent} and g_{vent}, were introduced to describe the performance of ventilated PV facades integrated into buildings, and the estimation of these parameters were also investigated [14]. In order to size air-conditioning equipment, procedures were developed for calculating hourly SHGFs on horizontal and vertical surfaces in Hong Kong where solar heat gain through fenestrations is often the largest component of the building envelope cooling load [15–17]. When referring to different kinds of windows, a comparison between calculated and measured SHGC for complex

fenestration systems was conducted [18], and the modeling of the heat and radiation transfer through the composite PCM-filled window and its optical investigation were investigated [19]. In summary, these researches dealt with the situations of windows with different structures, employed for different buildings and under different climates, but few of them were concerned about the case of employing both Trombe wall and fenestration.

Moreover, most wall materials may have considerable heat storage capacity, more or less. Hence, considering both fenestration and heat storage, the PV-TW wall installed in a fenestrated room with heat storage is theoretically and experimentally investigated in this paper. Based on our previous model [9], the PV-TW room's calculation is updated by the method of using the solar heat gain factor and overall heat loss coefficient. This paper, mainly, aims at validating the updated theoretical model by experiments and investigating the performance of this system such as the electrical generation and indoor temperature rise. In addition, the effect of heat storage on indoor temperature is also covered.

2. Description of the PV-Trombe wall and experimental methodology

The PV-Trombe wall system, as shown in Fig. 1, is composed of a PV glass panel on which some PV cells are affixed, a blackened wall acting as a thermal absorber and an air duct in between. There are also two air vents for winter heating and two air vents for summer cooling. In addition, it is noticeable that the PV glass panel consists of five layers from outside to inside: glass, EVA1, PV cell, EVA2 and TPT, respectively. The PV-TW wall system works as the original Trombe wall, and its detailed description can be found in [9].

Nevertheless, fenestration is generally considered in most practical rooms, while most wall materials may have considerable heat storage capacity, more or less. In order to test the performance of the PV-TW installed in a fenestrated room with heat storage, a comparable hot-box with two fenestrated rooms was used for performance comparison. Otherwise, the light weight walls of the comparable hot-box were short of heat storage capacity, thus 400 pieces of bricks were stacked in each room, in order to simulate practical rooms. The plan view of the hot-box is shown in Fig. 2 to illustrate the window and bricks well.

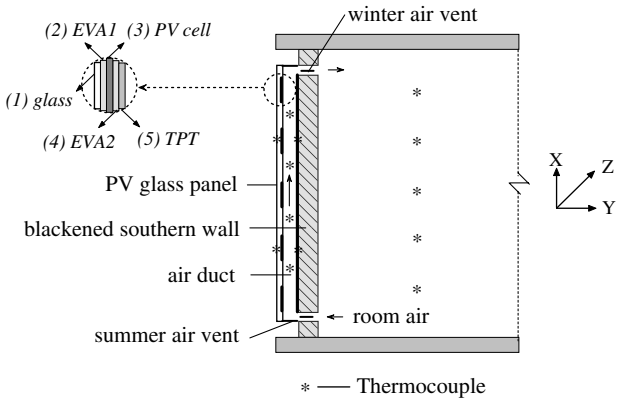

Fig. 1. Schematic diagram of PV-Trombe wall for winter heating and some important thermocouples.

Both rooms are of dimensions 2.66 m (height X coordinate) × 3.00 m (width Z coordinate) × 3.00 m (long Y coordinate) and the room walls' thicknesses are entirely 0.10 m. The PV-TW on the southern wall, which is located at 0.27 m from the western interior wall, consists of a PV glass panel with an area of 2.66 m (height) × 0.84 m (width) and a thickness of 5 mm, a matt black painted wall and an air duct with a depth of 0.18 m in between. Two winter air vents (0.40 m width × 0.10 m height) are located at 0.07 m from the ceiling and the floor. The double glazing window, which is located at 0.60 m from the eastern interior wall, is of dimensions 1.20 m (height) × 1.20 m (width).

A list of the key apparatus used in the current study is given in Table 1 and the locations of some important thermocouples are also schemed in Fig. 1. All measurements were carried out within a four-month period from

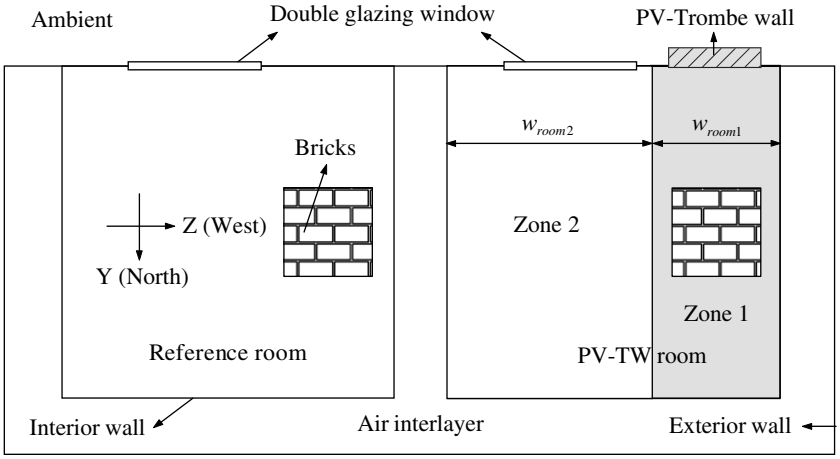

Fig. 2. The plan view of the hot-box showing the two fenestrated rooms with bricks.

Table 1
The list of experimental devices

Apparatus	Type	Number	Function	Specification
PV cell	Polycrystalline silicon, 5 cm × 5 cm in size	288	To generate electricity from the captured solar radiation	Area = 0.72 m^2, with 14% light-to-current conversion efficiency at standard conditions, and peak power at 100.8 W_p
Converter	JHQM-102D	1	To convert DC current to AC current	Input 48 V DC current; output 220 V, 50 Hz AC current
Storage battery	Lead-acid battery	4	To store electrical energy	12 V, 65AH, connection in series
Thermocouple	Copper-constantan		To measure temperature	Kept at 0 °C, measured accuracy within ±0.2 °C
Pyranometer	TBQ-2	1	To measure the incoming global solar radiation	Kept to the same South-facing vertical surface position as the PV-Trombe wall
Voltage sensor	WBV344S1	1	To measure the DC voltage of PV cells	
Current sensor	WBI224S1	1	To measure the DC current of PV cells	
Data logger	Agilent 34970 A	1	To record the measured data	Every 5-min intervals record
Computer	Desktop computer	1	To facilitate data logging	

December 2004 to March 2005 in Hefei, China. Through the transmission of the performance data via signal wirings to a data acquisition system, the performance data of the PV-TW was monitored and recorded all day at every 5 min interval. There were commonly three sunny days at each test trial to illustrate the performance well, and both the two winter air vents were periodically opened from 9:00 to 17:00. The experimental work reported here was the best result filtrated from the results during the four-month period.

3. System modeling

The detailed model of an original PV-TW, which includes the two-dimensional PV glass panel model, one-dimensional heat transfer models in the air duct, southern wall and room, has been given in our former paper [9]. However, due to the introduction of fenestration and heat storage in this paper, the heat transfer model in the room has great differences and will be emphasized here. Furthermore, the two-dimensional PV glass panel model will be updated when considering the effect of the incident angle on the transmissivity of glass.

3.1. Heat transfer on the PV glass panel

Due to the different absorptivities of the elements with and without PV cell on the PV glass panel, the heat transfer on the PV glass panel is considered to be a two dimensional problem (X and Z direction). Since the heat capacity of the flimsy PV cells is neglected, the energy balance can be obtained as follows:

$$\rho_G c_G \frac{\partial T_p}{\partial t} = \frac{\partial}{\partial X}\left(\lambda_G \frac{\partial T_p}{\partial X}\right) + \frac{\partial}{\partial Z}\left(\lambda_G \frac{\partial T_p}{\partial Z}\right) + \frac{b}{\delta_G} \quad (1)$$

where: $b = S_c + S_p T_p$, $S_P = -(h_{co} + \xi_1 h_{ro} + h_{ci} + \xi_2 h_{ri})$

(1) for the elements with PV cell on the glass panel:

$$S_c = \alpha_{WPV} G - E + h_{co} T_e + \xi_1 h_{ro} T_e + h_{ci} T_a + \xi_2 h_{ri} T_{wo}$$

(2) for the elements without PV cell on the glass panel:

$$S_c = \alpha_{NPV} G + h_{co} T_e + \xi_1 h_{ro} T_e + h_{ci} T_a + \xi_2 h_{ri} T_{wo}$$

where α_{WPV}, α_{NPV} are the equivalent absorptivities of the elements with and without PV cell on the glass panel, respectively. They can be calculated by the ray-tracing method as follows [20]

$$\alpha_{WPV} = \alpha_{PV}\tau_{PV} + (1 - \tau_{PV}) + \tau_{PV}(1 - \alpha_{PV})(1 - \tau_{PV}) \quad (2)$$

$$\alpha_{NPV} = (1 - \tau) + \tau(1 - \alpha_{wall})(1 - \tau) \quad (3)$$

where α_{PV}, τ_{PV}, τ are the absorptivities of PV cells, the transmissivity of the PV cell's outside layers (glass and EVA1 layers in Fig. 1) and the transmissivity of the elements without PV cell on the glass panel, which include glass, EVA1, EVA2, TPT layers, respectively; E is the electrical power rate generated by PV cells (W/m^2)

$$E = G_{PV} \cdot \eta_0 \cdot [1 - 0.0045(T_p - 25)] \quad (4)$$

where G_{PV} is the solar radiation which arrives on the PV surface through the glass and EVA1 layers (W/m^2), $G_{PV} = G \cdot \tau_{PV}$; η_0 is the electrical efficiency under standard conditions (1000 W/m^2, 25 °C), 14% is adopted in this paper.

If the effect of the time-dependant incident angle θ on the transmissivities is taken into account, a modified coefficient $K_{\tau\alpha}$ is introduced [20]

$$\tau = \tau_0 \cdot K_{\tau\alpha}, \quad \tau_{PV} = \tau_{PV0} \cdot K_{\tau\alpha}$$
$$K_{\tau\alpha} = 1 - 0.1 * \left(\frac{1}{\cos\theta} - 1\right) \quad (5)$$

where τ_{PV0}, τ_0 are the transmissivities when incident angle is zero, whose values are 0.81 and 0.60, respectively, if considering the transmissivities of different layers, as well as the PV glass inside and outside surfaces', dirty.

3.2. Heat transfer in the air duct

It is assumed that the air temperature in the air duct varies along the vertical direction X only, and then the heat transfer in the air duct is as follows:

$$\rho D c_p \frac{\partial T_a}{\partial t} = h_{ci}(T_p - T_a) + h_{wo}(T_{wo} - T_a) - \rho V_a D c_p \frac{\partial T_a}{\partial X} \quad (6)$$

$$V_a = \sqrt{\frac{0.5 \times g\overline{\beta} \cdot (T_{out} - T_{in}) \cdot L}{C_f \frac{L}{d} + \frac{C_{in} A_S^2}{A_V^2} + \frac{C_{out} A_S^2}{A_V^2}}} \quad (7)$$

3.3. Heat transfer across the southern wall

The southern wall comprises the PV-TW part and the rest part which is regarded as the normal wall part. It is assumed that the heat transfer across the southern wall is one-dimensional. The unsteady heat conduction equation is as follows:

$$\frac{\partial T_w}{\partial t} = \frac{\lambda_w}{\rho_w c_w} \frac{\partial^2 T_w}{\partial Y^2} \quad (8)$$

while its boundary conditions for different parts are as follows:

(1) for the PV-TW part

$$-\lambda_w \left(\frac{\partial T_w}{\partial Y}\right)_{y=0} = h_{wo}(T_{wo} - T_a) + \xi_3 h_{rwo}(T_{wo} - T_p)$$

$$+ G\alpha_{wall}\tau_{NPV}(1-\varepsilon) - \lambda_w \left(\frac{\partial T_w}{\partial Y}\right)_{y=D_w} = h_{wi}(T_{wi} - \overline{T_r})$$

(2) for the normal wall part

$$-\lambda_w \left(\frac{\partial T_w}{\partial Y}\right)_{y=0} = h_{nwo}(T_{nwo} - T_e) + \xi_1 h_{nrwo}(T_{nwo} - T_e) + G\alpha_{nwall}$$

$$-\lambda_w \left(\frac{\partial T_w}{\partial Y}\right)_{y=D_w} = h_{nwi}(T_{nwi} - \overline{T_r})$$

where α_{wall}, α_{nwall} are the absorptivities of the blackened wall and normal wall, respectively; ε is the ratio of PV cell coverage.

3.4. Heat transfer in the PV-TW room

Since the thermosiphon induces the indoor air flow from the top down, it has been assumed that the temperature in the PV-TW room varied along the vertical direction X only in our former paper [9]. However, as a window is introduced, the solar radiation can strike the indoor floor or its adjacent walls, so these walls are heated up, and an air flow from the bottom up occurs. Consequently, the flow in the PV-TW room becomes a mixed flow, which is hard to solve. In addition, with the bricks being affiliated, the effect of their heat storage on the heat transfer and flow problems in the PV-TW room should also be taken into account. Therefore, the one-dimensional assumption is no longer valid for this intricate problem, unless some simplifications are introduced. Considering that the average indoor temperature is the focus in engineering, the following simplifying assumptions are made and the processes of calculation are as follows:

1. The PV-TW room is divided into two zones by a face normal to the Z coordinate, as shown in Fig. 2, i.e. the western zone 1 and the eastern zone 2, as the solar radiation mostly strikes into zone 2 and the natural convection is relatively weak.
2. The heat transfer in zone 1 is also considered to be one-dimensional and the brick stack is converted to be a brick wall of dimensions L (height) $\times$ w_{room1} (width) $\times$ δ_b (long $\delta_b = 0.15$ m), with air flows washing its southern and northern sides. The air temperature in zone 1 can then be calculated from

$$\rho c_p L_{room} \frac{\partial T_{r1}}{\partial t} = \frac{A_{j1}}{w_{room1} \cdot L} \cdot U_j(T_j - T_{r1}) + R_{Trombe1} \cdot h_{wi}(T_{wi} - T_{r1}) + (1 - R_{Trombe1}) \cdot h_{nwi}(T_{nwi} - T_{r1}) - \frac{\dot{m} c_p}{w_{room1}} \cdot \frac{\partial T_{r1}}{\partial X} + h_{bo}(T_{bo} - T_{r1}) + h_{bi}(T_{bi} - T_{r1}) \quad (9)$$

where T_{r1} is the air temperature of zone 1 (°C); w_{room1} is the width of zone 1 (m); A_{j1} is the surface area of zone 1 except the southern and eastern surfaces (m^2); U_j is the overall heat transfer coefficient between air interlayer and indoor room (W/m^2 K); $\dot{m}$ is the mass flow rate ventilated from the top vent (kg/s); $R_{Trombe1}$ is the ratio between the area of PV-Trombe wall and the southern wall area of zone 1 i.e. $R_{Trombe1} = w/w_{room1}$; h_{bo}, h_{bi} are the heat transfer coefficients on the southern and northern surfaces of the converted brick wall, respectively (W/m^2 K); T_{bo}, T_{bi} are the temperatures of the southern and northern surfaces of the converted brick wall, respectively (°C).
3. The heat transfer in zone 2 is calculated by heat gain from all surfaces except the western surface adjacent to zone 1. The heat gain through the window is calculated by the solar heat gain factor and U-value as follows:

$$\rho c_p V_2 \frac{\partial T_{r2}}{\partial t} = A_{j2} U_j(T_j - T_{r2}) + h_{nwi}(T_{nwi} - T_{r2})(w_{room2} \cdot L - A_{window}) + A_{window}[g_w \cdot G + U_w(T_e - T_{r2})] \quad (10)$$

where T_{r2} is the air temperature of zone 2 (°C); w_{room2} is the width of zone 2 (m); V_2 is the volume of zone 2 i.e. $V_2 = w_{room2} \times L \times L_{room}$ (m^3); A_{j2} is the surface area of zone 2 except the southern and western surface (m^2); A_{window} is the area of window (m^2); g_w is the solar heat gain factor of window $g_w = 0.72$ [21]; U_w is the overall loss coefficient of window, when considering the heat loss of frames, $U_w = 4.2$ W/m^2 K [22].
4. At last, the temperature of the PV-TW room, which consists of zone 1 and zone 2, can be obtained by the weighted average method:

$$T_r = (w_{room1} \cdot T_{r1} + w_{room2} \cdot T_{r2})/(w_{room1} + w_{room2}) \quad (11)$$

4. Simulated results and experimental validation

The model as described above has been validated against experimental data by using three days time records in Hefei (February 19–21, 2005). The time step was 10 s, starting at 1:00. The corresponding ambient conditions are shown in Fig. 3. The initial conditions are initialized according to the measured values at that time. The material properties used in this paper are listed in Table 2 and then the following results, which can be representative for the system's temperature distribution and electrical performance, are obtained to compare the simulated and experimental results, as well as to analyze the system's performance: average temperatures of the elements with and without PV cell on the glass panel (denoted by T-PB, T-PW, respectively), average air temperature in the air duct (T-A), average temperature of the outside and inside of the blackened southern wall (T-WO, T-WI, respectively), average indoor temperature in the PV-TW room (T-R), electrical power (P) and efficiency (EFF). Subsequently, the simulated and experimental results are illustrated in the following figures, where '*S*' and '*E*' mean the simulated and experimental results, respectively. In addition, it is also shown in the figures that the simulated and experimental results are illustrated by dashed and solid lines, no matter what color they are.

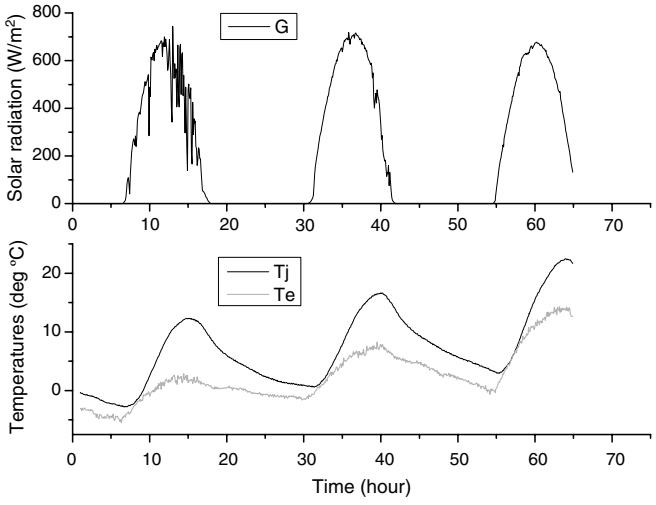

Fig. 3. The ambient conditions during February 19–21, 2005.

The three-day temperatures of the PV-TW installed in a fenestrated room with heat storage are shown in Figs. 4–8. Taking one with another, the simulated and experimental results are found in good agreement, except that the temperatures of the different elements on the PV glass panel are only found in reasonable agreement. These contrasts are generally due to the approximate value taken for thermophysical parameters used in the simulation, and the assumptions in the model. Furthermore, following additional comments on these results can be given as follows:

1. The temperatures of the different elements on the PV glass panel are shown in Fig. 4. The temperature difference between T-PB and T-PW reflects the different absorptivities between the elements with and without PV cells in some extent.
2. Some fluctuations on every day's 9 o'clock for the experimental temperatures in the air duct, as shown in Fig. 5, are mostly due to the sudden injection of hot air flow when the vents are open.
3. The temperatures of outside and inside surface of the blackened southern wall are shown in Figs. 6 and 7, respectively. The high temperature on the outside of the blackened southern wall, as a result of its high absorptivity, mainly lies on the ratio of PV cell coverage. The bigger the ratio is, the lower the T_{wo} is. In addition, the well consistent simulated and experimental T_{wo} and T_{wi} can characterize the temperature distribution on the blackened southern wall well.
4. The simulated and experimental indoor temperatures, as shown in Fig. 8, are found in good agreement. However, the calculation of the heat transfer in zone 2, using SHGF and *U*-value, is an instantaneous heat gain method, without regard to the heat storage effect of the walls. It is the small heat storage of this kind of light weight material that leads to a better agreement. Otherwise, another remarkable observation in this figure is the escalating troughs during the 3 days as a result of the heat storage function of bricks, even if it is not effective enough. Hence, it is necessary to setup heat storage to prevent a steep drop of the indoor temperature at night.

A relativeness index, defined as the temperature difference between average indoor temperature and ambient, was introduced [23] as tests would have to be done on different days. Two different relativeness indexes, namely the

Table 2
The material properties

Material	Density (kg/m^3)	Specific heat (J/kg K)	Thermal conductivity (W/m K)	Specification
Air	1.18	1000	0.026	The kinematic viscosity is 1.58×10^{-5} m^2/s
Glass panel	2515	810	1.4	The ratio of PV cell coverage is 0.324, the absorptivity of PV is 0.9
Wall	70	1045	0.026	The absorptivity of the blackened wall and normal wall part is 0.9 and 0.48, respectively
Brick	1800	840	0.814	400 pieces

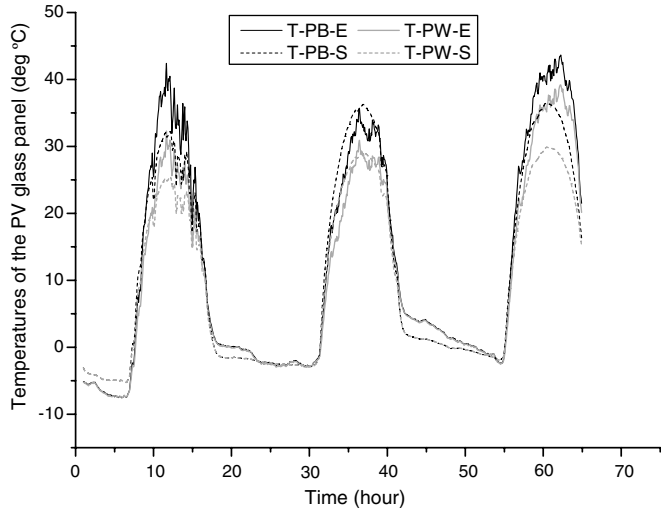

Fig. 4. The temperatures of the different elements on the PV glass panel.

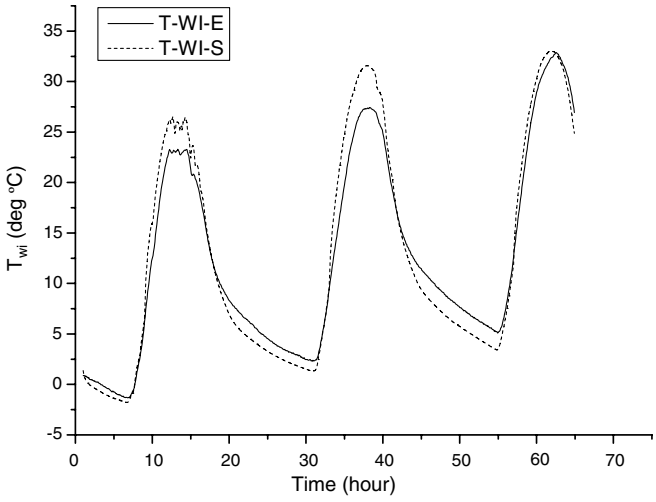

Fig. 7. The temperature of the inside surface of the blackened southern wall.

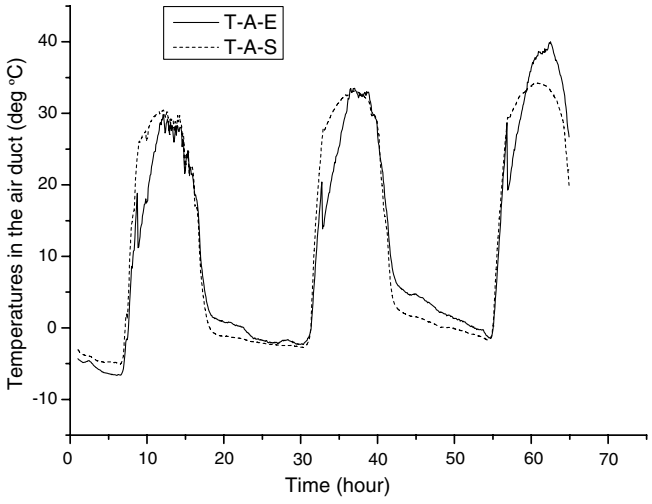

Fig. 5. The temperature in the air duct.

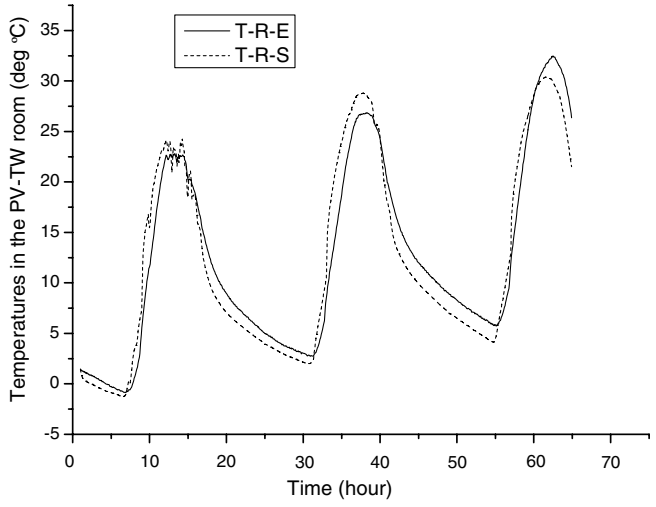

Fig. 8. The temperature in the PV-TW room.

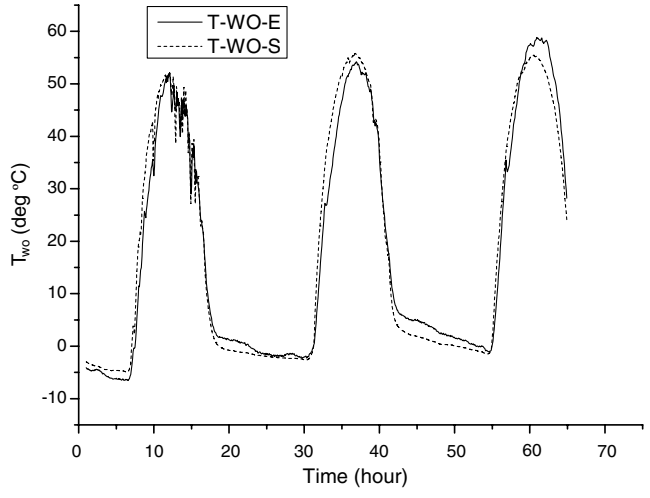

Fig. 6. The temperature of the outside surface of the blackened southern wall.

temperature difference between PV-TW room and ambient, as well as that between the PV-TW room and the reference room, are defined in this paper, which are denoted by RI-A, RI-R, respectively. As shown in Fig. 9, the maximum RI-A can reach 21.3 °C while the RI-R can culminate at 7.7 °C, which can be considered to be a significant temperature elevation since the PV-TW only occupies 28% of the southern wall.

The average electrical efficiency is defined as follows:

$$\bar{\eta} = \bar{E}/\bar{G} = \sum E \Big/ \sum G \tag{12}$$

The daily (February 21, 2005) simulated and experimental electrical power and efficiency are shown in Figs. 10 and 11, respectively. It can be seen the simulated electrical performances can agree well with the experimental results, except the electrical efficiency before 9:00. This is because that the measurement errors are relatively bigger if compared with

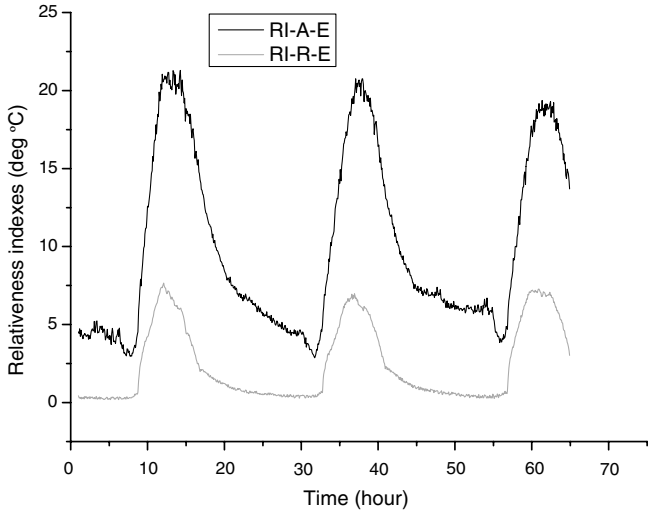

Fig. 9. Two different relativeness indexes.

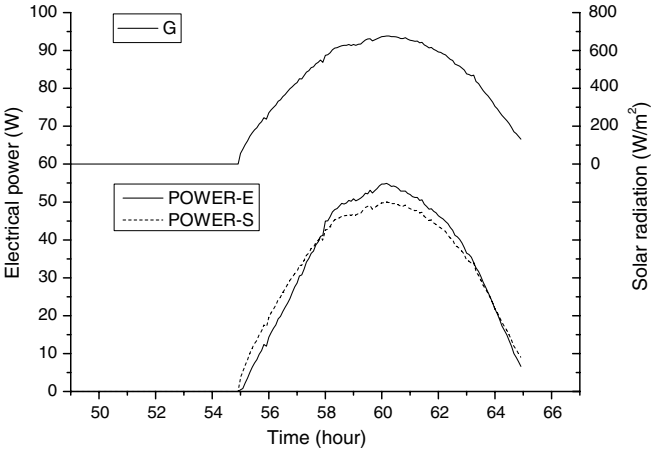

Fig. 10. The electrical power on February 21, 2005.

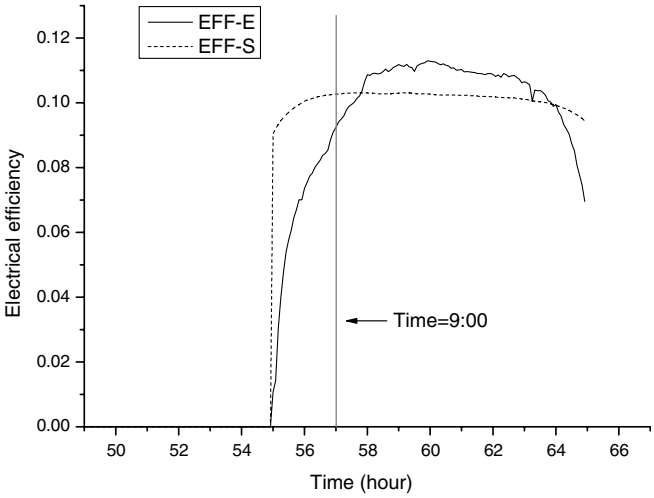

Fig. 11. The electrical efficiency on February 21, 2005.

the small testing values before 9:00, and electrical efficiency is a relative quotient. In other words, the absolute error is small while the relative error may be much bigger. Besides, the gradual mismatch of Eq. (5) when the incident angle is bigger than 60° is another latent reason. The statistic of experimental results during day time (7:00 –17:00) shows that the daily average power can reach 35.4 W, with an average efficiency of 10.4% when the average solar radiation and ambient temperature are 475 W/m^2 and 9.7 °C, respectively.

5. Conclusion

A simplified mathematical model for PV-TW, in the special case of being installed in a fenestrated room with heat storage, has been updated based on our previous model, and field testing in this case is also carried out to validate the model. At last, an overall comparison between simulated and experimental results has been performed and the comparative study gives the following results:

1. In general, the simulated and experimental results are found in good agreement, which indicates that the updated model is valid in the special case.
2. From the view of field testing, a significant indoor temperature increase with a maximum of 7.7 °C, if compared with the reference room, can be obtained by the PV-TW installed in a fenestrated room with heat storage. Meanwhile, the average electrical efficiency can reach 10.4%.
3. The comparison between simulated and experimental results shows a good prediction capability of the simple updated model. Hence, the model can be used to predict this PV-TW system's performance at different climatic and design conditions, and to size the components of the system for optimizing the system. Thereby, with this theoretical support, the applications of PV-TW will be more feasible, especially in areas with good solar energy resources and winter heating requirement, such as Tibet, China.

Nevertheless, some part of the model is too simplified to match the testing results well. Thus, a more detailed model should be expanded. There are also problems such as the material is different from concrete used in practical buildings, so the performances of PV-TW with different materials deserve further theoretical and experimental researches.

Acknowledgement

The study was sponsored by

(1) National Science Foundation of China (NSFC), Project Number: 50408009.
(2) Research Center for Photovoltaic System Engineering, Ministry of Education, China.

References

[1] Guohui Gan, A parametric study of Trombe walls for passive cooling of buildings, Energy and buildings 27 (1) (1998) 37–43.

[2] Z. Zrikem, E. Bilgen, Theoretical study of a compositive trombe-michel wall solar collector system, Solar Energy 39 (5) (1987) 409–419.

[3] L. Zalewski, M. Chantant, Experimental thermal study of a solar wall of composite type, Energy and Buildings 25 (1) (1997) 7–18.

[4] P. Raman, Sanjay Mande, V.V.N. Kishore, A passive solar system for thermal comfort conditioning of building in composite climates, Solar Energy 70 (4) (2000) 319–329.

[5] He Wei, Ji Jie, Zhang Aifeng, Pei Gang, Dong Jun, Cheng Hongbo, Experimental test and data analyze of thermal performance of a solar house with improved Trombe wall, Journal of University of Science and Technology of China 33 (5) (2003) 567–572.

[6] Ye Hong, Ge Xinshi, Dynamic simulation of several solar houses with different composite Trombe–Michel wall and the compare of their thermal performances, Acta Energiae Solaris Sinica 21 (4) (2000) 349–357.

[7] Joachim Benemann, Oussama Chehab, Eric Schaar-Gabriel, Building-integrated PV modules, Solar Energy Materials and Solar Cells 67 (1–4) (2001) 345–354.

[8] H. Maurus, M. Schmid, B. Blersch, P. Lechner, H. Schade, PV for Buildings- Benefits and experiences with amorphous silicon in BIPV applications, Refocus 5 (6) (2004) 22–27.

[9] Ji Jie, Yi Hua, He Wei, Pei Gang, Lu Jianping, Jiang Bin, Modeling of a novel Trombe wall with PV cells, Building and Environment, in press.

[10] K.A.R. Ismail, J.R. Henriquez, Modeling and simulation of a simple glass window, Solar Energy Materials and Solar Cells 80 (3) (2003) 355–374.

[11] M. Cucumo, D. Kaliakatsos, V. Marinelli, Estimating effective solar absorptance in rooms, Energy and Buildings 23 (2) (1995) 117–120.

[12] M.S. Bhandari, N.K. Bansal, Solar heat gain factors and heat loss coefficients for passive heating concepts, Solar Energy 53 (2) (1994) 199–208.

[13] N.K. Bansal, Shail, R.C. Gaur, Application of U and g values for sizing passive heating concepts, Solar Energy 57 (5) (1996) 361–373.

[14] L. Mei, D. Infield, U. Eicker, V. Fux, Parameter estimation for ventilated photovoltaic facades, Building Services Engineering Research and Technology 23 (2) (2002) 81–96.

[15] Danny H.W. Li, Joseph C. Lam, Solar heat gain factors and the implications to building designs in subtropical regions, Energy and Buildings 32 (1) (2000) 47–55.

[16] Danny H.W. Li, Joseph C. Lam, Development of solar heat gain factors database using meteorological data, Building and Environment 36 (4) (2001) 469–483.

[17] Danny H.W. Li, Joseph C. Lam, Analysis of solar heat gain factors using sky clearness index and energy implications, Energy Conversion and Management 42 (5) (2001) 555–571.

[18] Joseph H. Klems, Jeffrey L. Warner, Guy O. Kelley, Comparison between calculated and measured SHGC for complex fenestration systems, ASHRAE Transactions 102 (1) (1996) 931–939.

[19] K.A.R. Ismail, J.R. Henriquez, *U*-values, optical and thermal coefficients of composite glass systems, Solar Energy Materials and Solar Cells 52 (1–2) (1998) 155–182.

[20] J.A. Duffie, W.A. Beckman, Solar Engineering of Thermal Processes, second ed., John Wiley & Sons, INC, 1991.

[21] GANA. Specifiers Guide to Architectural Glass, 2005 Edition.

[22] Dianhua Xue, Air conditioning (in Chinese), Tsinghua University Press, 1991.

[23] Joseph Khedari, Boonlert Boonsri, Jongjit Hirunlabh, Ventilation impact of a solar chimney on indoor temperature fluctuation and air change in a school building, Energy and Building 32 (1) (2000) 89–93.